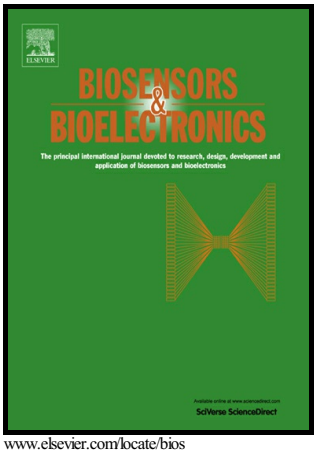

www.elsevier.com/locate/bios

Hybrid organic/inorganic interfaces as reversible label-free platform for direct monitoring of biochemical interactions

Tatiana P. Vello, Larissa M.B. da Silva, Gustavo O. Silva, Davi H.S. de Camargo, Cátia C. Corrêa, Carlos C. Bof Bufon

PII: S0956-5663(16)30805-3
DOI: http://dx.doi.org/10.1016/j.bios.2016.08.050
Reference: BIOS9047

To appear in: *Biosensors and Bioelectronic*

Received date: 1 June 2016
Revised date: 5 August 2016
Accepted date: 16 August 2016

Cite this article as: Tatiana P. Vello, Larissa M.B. da Silva, Gustavo O. Silva, Davi H.S. de Camargo, Cátia C. Corrêa and Carlos C. Bof Bufon, Hybri organic/inorganic interfaces as reversible label-free platform for direct monitorin of biochemical interactions, *Biosensors and Bioelectronic* http://dx.doi.org/10.1016/j.bios.2016.08.050

Hybrid organic/inorganic interfaces as reversible label-free platform for direct monitoring of biochemical interactions

Tatiana P. Vello[a,b], Larissa M. B. da Silva[a], Gustavo O. Silva[a], Davi H. S. de Camargo[a], Cátia C. Corrêa[a], Carlos C. Bof Bufon[a,b,c*]

[a]Brazilian Nanotechnology National Laboratory (LNNano), CNPEM, 13083-970, Campinas, Brazil.

[b]Department of Physical Chemistry, Institute of Chemistry, University of Campinas, P.O. Box 6154, 13084-862 Campinas, SP Brazil.

[c]Institute of Physics "Gleb Wataghin" (IFGW), UNICAMP, 13083-859, Campinas, Brazil.

[*]Corresponding author. cesar.bof@lnnano.cnpem.br

Abstract

The combination of organic and inorganic materials to create hybrid nanostructures is an effective approach to develop label-free platforms for biosensing as well as to overcome eventual leakage current-related problems in capacitive sensors operating in liquid. In this work, we combine an ultra-thin high-k dielectric layer (Al_2O_3) with a nanostructured organic functional tail to create a platform capable of monitoring biospecific interactions directly in liquid at very low analyte concentrations. As a proof of concept, a reversible label-free glutathione-S-transferase

(GST) biosensor is demonstrated. The sensor can quantify the GST enzyme concentration through its biospecific interaction with tripeptide reduced glutathione (GSH) bioreceptor directly immobilized on the dielectric surface. The enzymatic reaction is monitored by electrical impedance measurements, evaluating variations on the overall capacitance values according to the GST concentration. The biosensor surface can be easily regenerated, allowing the detection of GST with the very same device. The biosensor shows a linear response in the range of 200 pmol.L^{-1} to 2 µmol.L^{-1}, the largest reported in the literature along with the lowest detectable GST concentration (200 pmol.L^{-1}) for GST label-free sensors. Such a nanostructured hybrid organic-inorganic system represents a powerful tool for the monitoring of biochemical reactions, such as protein-protein interactions, for biosensing and biotechnological applications.

Keywords: Hybrid organic-inorganic nanostructures, solid-liquid interfaces, biosensor, glutathione S-transferase.

1. Introduction

The combination of materials of different nature and dimensionalities to form functional elements is an effective approach to address sensing- and biosensing-related challenges (Zheng et al., 2005; Lin et al., 2009; Stern et al., 2007). The immobilization of organic layers on nanostructured materials such as silicon nanowires (Ahn et al., 2010; Gao et al., 2010), semiconducting layers (Ashkenasy et al., 2002; Casalini et al., 2015; Bof Bufon et al., 2011), carbon nanotubes (Lin et al., 2004; Nguyen et al., 2002), high-k oxides films (Bof Bufon et al., 2010; Vervacke et al., 2014, 2012) and, more recently, graphene (Liu et al., 2012; Shan et al., 2009) has been recognized as key to produce devices with novel functionalities and improved performance. In sensing and biosensing, additional advantage is achieved by making use of

solid-liquid interfaces for the detection of specific analytes. Insulator/electrolyte (Bousse and Bergveld, 1983) interfaces, for instance, have been widely exploited in transistor-like structures for the detection/monitoring of organic solvents (Grimm et al., 2013), heavy metal ions (Cobben et al., 1992) and biomolecules (Cui, 2001), to mention a few. In order to use such interfaces to target specific molecules, receptor elements are immobilized on top of the insulating layer (Berggren et al., 2001; Cui, 2001).

In capacitive sensors, the observation of changes in the solid/liquid interface requires the capacitance of the insulating layer to be as high as possible (Berggren et al., 2001). This strategy is adopted to enhance the capability of measuring the changes on the electrical double layer capacitance as a result of recognition events occurring at the solid/liquid interface. Consequently, to monitor the concentration of specific analytes in this type of devices, which is proportional to the charge density at the interface, the sensor has to operate at low frequencies (< 100 Hz) (Taylor and Macdonald, 1987), which is known to be unstable (Maupas et al., 1997). The incorporation of insulating organic molecules on top of conducting substrates has also been investigated and modeled (Finklea et al., 1993; Góes et al., 2012). Nevertheless, the permeability of the organic tail to the plethora of ions present in solution may bring serious instabilities to device operation (Góes et al., 2012).

The understanding of biochemical interactions is also of fundamental importance for both biosensor's development and the identification of biological mechanisms responsible for a set of physiological activities. Reduced glutathione (GSH), for instance, is an ubiquitous tripeptide associated with vital functions in the body, including the regulation of cell's redox system (Martos-Maldonado et al., 2015). The protection of cells against damage occurs via a detoxification process driven by the conjugation of GSH with xenobiotics, which is mediated by

the glutathione S-transferase (GST) enzyme (Martos-Maldonado et al., 2015, 2012). In this sense, the GSH/GST pair is key for detecting different exogenous substances, such as herbicides and insecticides (Kapoli et al., 2008), fungicides (Singh et al., 2009) and anticancer drugs (Materon et al., 2014). Furthermore, the GSH concentration, along with the GST expression and activity, have been associated to the neurodegenerative diseases like Parkinson's and Alzheimer's (Liu et al., 2015; Mazzetti et al., 2015). In addition, variable expressions of GST have been correlated to various types of cancer (Chuang et al., 2005), as well as to the capability of cells to respond to anticancer drugs (Townsend and Tew, 2003; Tsuchida and Sato, 1992). In all cited cases, the evaluation methodology consists on comparing healthy and pathological cells, where the relative changes of GSH and GST quantities are of interest.

Complexes or labeled methods of analysis, such as radioimmunoassays (Howie et al., 1989), gene chips (Chuang et al., 2005) and ELISA (Daukantienė et al., 2014) are usually employed to follow the probe/target molecule interaction. These methods, however, usually cannot provide real time measurements, are more expensive and bulkier then label-free systems (Tsouti et al., 2011). The development of a label-free GST biosensor, i.e., an analytical device to directly monitor the presence of the target molecule (GST) without requiring additional reagents, usually luminescent and electrochemical compounds, for signal generation, is a relevant case as a proof of concept for the monitoring of biochemical interactions. In the literature, just a very limited number of methods, including surface plasmon resonance (Jung et al., 2006), silicon nanowire field-effect transistors (Lin et al., 2009) and water-gated organic transistors (de Oliveira et al., 2016) have reported the label-free detection of GST. To the best of our knowledge, if all reported GST label-free sensors (Jung et al., 2006; Lin et al., 2009; Martos-Maldonado et al., 2012; Qin et al., 2015) are combined, GST can be monitored in a range of concentration of three orders of

magnitude (from 2×10^{-9} mol L^{-1} to 4.2×10^{-6} mol L^{-1}). In addition, most of these devices cannot be reused since they employ innovative but complexes functionalization methods that may lead to difficulties in obtaining reproducible manufacturing/regeneration processes (Ahn et al., 2010) as well as routes for GSH/GST monitoring that are not reversible (Jung et al., 2006; Martos-Maldonado et al., 2012; Qin et al., 2015).

In this work, we demonstrate a label-free, reversible and highly sensitive hybrid organic-inorganic biosensor to monitor GSH/GST at a wide range of GST concentration (from 200 pmol.L^{-1} to 2 μmol.L^{-1}). The sensor's architecture and operation rely on the combination of an ultra-thin high-k dielectric layer (3.3 nm Al_2O_3) with the functional bioactive tail to monitor variations of the net charge at the hybrid solid/liquid interface caused by the GSH/GST biospecific interaction. Here, the organic-inorganic combination allowed us to overcome two critical drawbacks in capacitive biosensors: a) the instabilities arising from low frequency operation (Maupas et al., 1997; Taylor and Macdonald, 1987) and b) the high ionic permeability of the biorecognition layer, which may lead to electrical instabilities and irreproducible measurements (Berggren et al., 2001). The conformational Al_2O_3 coating of metallic electrodes is capable of suppressing eventual leakage currents and enables the device to continuously operate in aqueous buffered medium.

The immobilization of biomolecules in biosensors and related biotechnological applications commonly utilizes functionalization agents bearing thiol and silane groups (Lin et al., 2009; Casero et al., 2002). Here, we employed an alternative functionalization route capable of delivering high quality self-assembled phosphonic acid monolayers (SAM) chemically bonded to the Al_2O_3 nanocoating. Such a layer is part of the organic functional tail of our device that allows the GSH immobilization. Once the functionalized device is exposed to the GST in aqueous

phosphate buffer solution (PBS), the GSH/GST reversible interaction can be precisely monitored. The very same biosensor was successfully employed to quantify the GST concentration from 200 pmol.L^{-1} to 2 μmol.L^{-1}; the broadest linear operation range reported so far to this enzyme. For comparison, even combining all label-free devices reported in literature, our device outperforms their operation range in one order of magnitude. In addition, to the best of our knowledge, we also achieved the lowest detectable concentration of GST (200 pmol.L^{-1}) among such devices (Jung et al., 2006; Lin et al., 2009). From the manufacturing point of view, the fabrication process is compatible with standard microfabrication techniques and the scaling-up production is simple and straightforward. Finally, the devices exhibited a stable operation, with the possibility of being constantly regenerated for further use.

2. Materials and methods

2.1. Fabrication of the biosensor's inorganic structure

The inorganic part of the device comprises nickel interdigitated electrodes, prepared by standard photolithography and thin-film deposition processes (see Section 1 and Fig. S1 in the Supplementary Material for details), coated with a conformational Al_2O_3 insulating layer. Therefore, the device's electrodes are protected from PBS used for the device functionalization and characterization. The gap between electrodes (~21 μm) is filled with PBS. In such a configuration, the device electrical impedance depends on the insulator thickness, the aqueous medium (PBS) ionic strength, and the device interfacial characteristics. The equivalent circuit shown in Fig. 1b represents the inorganic part of the device when exposed to the liquid medium. The modification created by the immobilization of the bioactive layer at the oxide surface is expected to induce changes in the electrical double layer capacitance (C_{dl}) at the solid/liquid

interface. Therefore, to assess such changes, the capacitance of the insulating layer (C_{ox}) has to be maximized. For simplicity, two variables were initially considered: the insulating layer a) dielectric constant (ε) and b) thickness (*d*). Here, we opted to use an ultrathin Al_2O_3 film deposited by atomic layer deposition (ALD) at 150°C as the device insulator. This choice is made based on the following reasons: firstly, ALD guarantees an excellent conformational coating within the monolayer precision level (Groner et al., 2004); secondly, amorphous Al_2O_3 layers with thicknesses smaller than 10 nm can exhibit both high ε (~9) and low leakage currents (Bof Bufon et al., 2010). Different from what has been recently reported (Correa et al., 2015), no signature of degradation of the Al_2O_3 nanocoating in the presence of aqueous solution was observed. Here, stability is achieved after conditioning the Al_2O_3 layer using an ac voltage with amplitude 5 times higher than the signal used to characterize the devices (200 mV). The procedure consists of immersing the Al_2O_3 coated interdigitated electrodes in PBS while applying 1 V to the devices pads. This process takes approximately 30 minutes and provides the stability necessary to operate the devices in aqueous medium (see Section 2 in the Supplementary Material).

2.2. Fabrication of the biosensor's organic tail

The device functionalization starts with the immersion of Al_2O_3 coated electrodes in a 5 mol L^{-1} solution of 2-aminoethylphosphonic acid prepared in deionized water for approximately 1 h. Next, the device is exposed to 1 mol L^{-1} solution of 3-maleimidobenzoic acid N-hydroxysuccinimide ester (MBS) prepared in ethanol for 2 h. The functionalization continues by immobilizing reduced glutathione (GSH) from a solution of 1 mol L^{-1} prepared in PBS (0.1 mol L^{-1}, pH 7.0) for 2 h. The target enzyme glutathione S-transferase (GST), > 25 U/mg, from equine liver (E.C. 2.5.1.18), was prepared in PBS (0.1 mol L^{-1}, pH 7.0) at different concentrations. The

exposure of GSH to GST takes ~1 h and it is performed at various concentrations of GST (from 200 pmol L^{-1} to 2 µmol L^{-1}). All chemicals were purchased from Sigma-Aldrich and used without further purification. A schematic diagram of the device functionalization steps and GST biorecognition is illustrated in Fig. 2. The biosensor electrical response was evaluated in 0.1 mol L^{-1} PBS using an Agilent E4980A Precision LCR Meter. The parallel capacitance (C_p) and resistance (R_p) values were analyzed in the frequency range of 20 Hz – 2 MHz with a sine-wave voltage signal amplitude of 200 mV. For measurements at a fixed frequency, an average of 90 points were collected during approximately 10 minutes.

3. Results and Discussion

3.1. *Evaluation of the oxide/liquid interface capacitance*

Fig. 1c presents the measured capacitance (C_p) as a function of the Al_2O_3 thickness for devices immersed in PBS. Considering the equivalent circuit presented in Fig. 1b, the measured capacitance (C_p) can be fit according:

$$\frac{1}{C_p} = \frac{1}{C_{dl}} + \frac{1}{C_{ox}} = \frac{1}{C_{dl}} + \frac{d}{\varepsilon\varepsilon_0 A} \qquad (1)$$

where ε_0 is the permittivity of the free space and A the electrode's area. The specific capacitance of the electrical double layer (C_{dl}/A) was found ~19µF/cm^2, in agreement with previously reported values (Bard and Faulkner, 2000). Here, it is worth mentioning that Al_2O_3 films are sufficiently thin to allow the formation of a non-negligible electrical double layer at the oxide/electrolyte interface even with the metallic electrode not being directly exposed to the electrolyte. From the insulator capacitance (C_{ox}), the value obtained for ε is 9±1, which agrees with previously reported data (Bof Bufon et al., 2010; Sharma et al., 2014). Since we are capable of experimentally retrieve both C_{dl} and ε, we can use such capacitor structure to evaluate

capacitance changes occurring at the oxide/dielectric interface as a result of the surface functionalization and the detection of analytes.

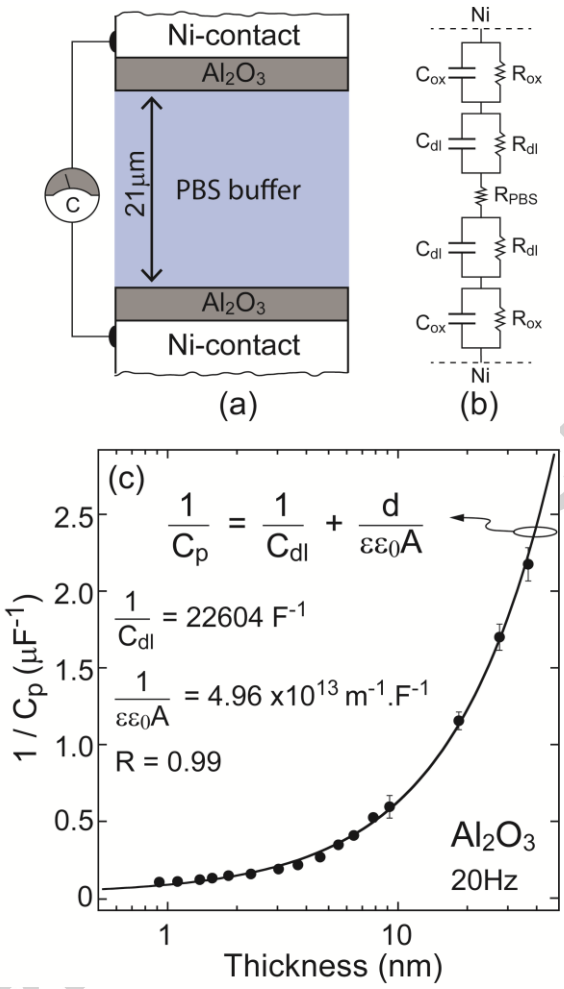

Fig. 1. (a) Schematics of the capacitor structure comprising interdigitated nickel electrodes coated by an Al_2O_3 conformational film (not to scale). The Al_2O_3 thickness varied from 0.9 to 36 nm. The gap between the electrodes is 21 µm. (b) Equivalent circuit of the structure described in (a); C_{ox} and C_{dl} are the capacitances of the oxide and electrical double layers, respectively. R_{ox} and R_{dl} refers to the respective resistances and R_{PBS} is the resistance associated to PBS (< 50 Ω). (c) C_p as a function of the Al_2O_3 thickness. From the data fit, using Eq. 1, C_{dl} was found equal to 44.2 µF and $\varepsilon \sim 9\pm1$ for $A = 2.37\pm0.05$ cm^2 ($C_{dl}/A \sim 19$µF/cm^2). The total Al_2O_3 thickness used in the biosensor is ~6.6 nm (3.3 nm covering each electrode). This value was defined evaluating the phase of the ac signal in combination

with the capacitance measurements shown in Fig. 1c (see Section 3 and Fig. S3 in the Supplementary Material).

3.2 Evaluation of the device functionalization tail

As described in the experimental section, the device functional tail is prepared in three steps (see Fig. 2b) namely: incorporation of phosphonic acid SAM on top of the Al_2O_3 surface (step I), MBS attachment (step II) and GSH immobilization (step III). Once the functional layer is assembled, the biosensor is exposed to GST as shown in Fig. 2c (step IV). The association and dissociation of the GSH/GST pair is known to be reversible (Glatz et al., 1997a). Such reversibility, illustrated in Fig. 2c (step V), was achieved by removing the GST enzyme with a highly concentrated washing solution of GSH (10 mmol L^{-1}), allowing the biosensor reutilization (Lin et al., 2009).

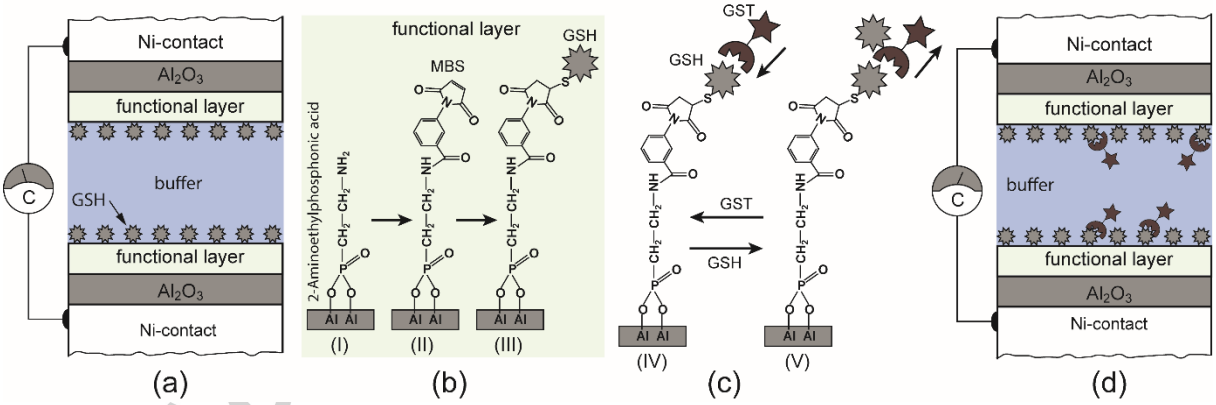

Fig. 2. (a) Device structure comprising the functional layer immobilized on a Al_2O_3-coated Ni film (3.3 nm) deposited by ALD. The functional layer (b) is formed by first modifying the Al_2O_3 surface with 2-aminoethylphosphonic acid SAM (I). Next, the MBS is linked (II) to allow the immobilization of GSH (III). (c) The GST enzyme interact with GSH (IV). (d) The GSH-GST interaction is detected at the biosensor surface and the resulting capacitance changes are recorded. The device regeneration occurs by rinsing the surface (c) with 10 mmol L^{-1} GSH solution, removing GST (step V). After rising, the structure returns to the original functional layer (a).

The functionalization steps and GSH/GST interaction were monitored by measuring both the capacitance (Fig. 3a) and the resistance (see Section 4 and Fig. S4 in the Supplementary Material) as a function of frequency. As shown in Fig. 3a, capacitance changes are verified at both low and high frequencies as the surface functionalization evolves. At low frequencies, due to the protonation of the phosphonic acid amino groups in PBS, the net amount of positive charges at the electrode's surface increases after step I (Lai et al., 2012). As a result, the electrode-electrolyte capacitance increases by ~80 μF at 20 Hz. The calculated amount of additional positive charges ($\Delta Q_a = \Delta C_a \cdot V_{ac}$) from the amino groups created at the surface is 16 μC. Considering one charge per molecule and an electrode area of ~0.250 cm^2, we estimate a surface coverage of ~4 x 10^{14} molecules/cm^2. This value corresponds to a molecular cross-sectional area of ~25 $Å^2$/molecule, which is in the range of values previously reported for organophosphonate monolayers (Hanson et al., 2003). After the functionalization steps II and III (MBS and GSH immobilization, respectively) such net amount of charges reduces, leading to a capacitance decrease. Finally, the exposure of the GSH layer to a 0.2 μmol L^{-1} GST solution (step IV in Fig. 2c) results in an increase of the capacitance at low frequencies (20 Hz). By applying the same evaluation method used above, the charge increment (ΔQ) at the electrode-electrolyte interface after the GSH/GST interaction (step III to IV) becomes 6.5μC. Even though GST is slightly negatively charged in PBS at pH 7.0 (GST isoelectronic point (Lin et al., 2009) is 6.7), after its interaction with the immobilized GSH the net amount of charge available at the device surface is still positive. This suggests that some GSH sites remain available for GST binding at such enzyme concentration.

At high frequencies (60 kHz), according to the theoretical model (Bousse and Bergveld, 1983) used to explain the electrical impedance of the electrolyte/insulator interface, the measured

capacitance is mainly a result of the insulating layer - the capacitance due to the electrical double-layer is disregarded. Therefore, in this regime, the device is modeled as a parallel plate capacitor where the geometrical capacitance is given by:

$$C = \frac{\varepsilon \varepsilon_0 A}{d} \qquad (2)$$

where ε is thin-film dielectric constant, ε_0 the permittivity of the free space, A is the electrode area and d the thin-film thickness. Again, we can retrieve the oxide dielectric constant ($\varepsilon = 9\pm1$) now from capacitance-frequency measurements. At the very same frequency, the capacitance obtained by immobilizing the aminophosphonic acid SAM (step I in Fig. 2b) on top of the Al_2O_3 surface (C_{pI}) decreases to 0.17 µF. Consequently, by considering the equivalent capacitance of the device immediately after the functionalization step I as:

$$\frac{1}{C_{pI}} = \frac{1}{C_{ox}} + \frac{1}{C_a} \qquad (3)$$

the capacitance of the amino molecule (C_a) can be obtained. By using the experimental values $C_{ox} = 0.27$ µF and $C_{pI} = 0.17$ µF, C_a is found equal to 0.46 µF, which correspond to a 0.7±0.2 nm thick aminophosphonic acid SAM, considering a dielectric constant of 2.5 - 3.0 (Bof Bufon et al., 2010; Góes et al., 2012) and a close-packed monolayer arrangement.

The inset of Fig. 3a shows the normalized capacitance (C_p/C_{GSH}) at both 20 Hz and 60 kHz. C_p is the capacitance measured after each functionalization step and C_{GSH} is the capacitance measured after GSH immobilization (step III). At 20 Hz, C_p/C_{GSH} increases from step 0 to I and drops as the functionalization evolves (from I to II and then to III). The 60 kHz trace exhibits a continuous decrease from 0 to III. Note that the changes in C_p/C_{GSH} observed for the GSH/GST interaction (step III to IV) are identical at both 20 Hz and 60 kHz. In principle, both frequencies can be used to probe the GSH/GST interaction. The differences lie in the manner the biosensor

operates. At low frequencies, the net amount of charges present at the device surface is essential to define the electrode-electrolyte capacitance. At high frequencies, however, the capacitance is mainly due to the dielectric properties of the immobilized molecular layers, since the electrical double-layer formation can be disregarded.

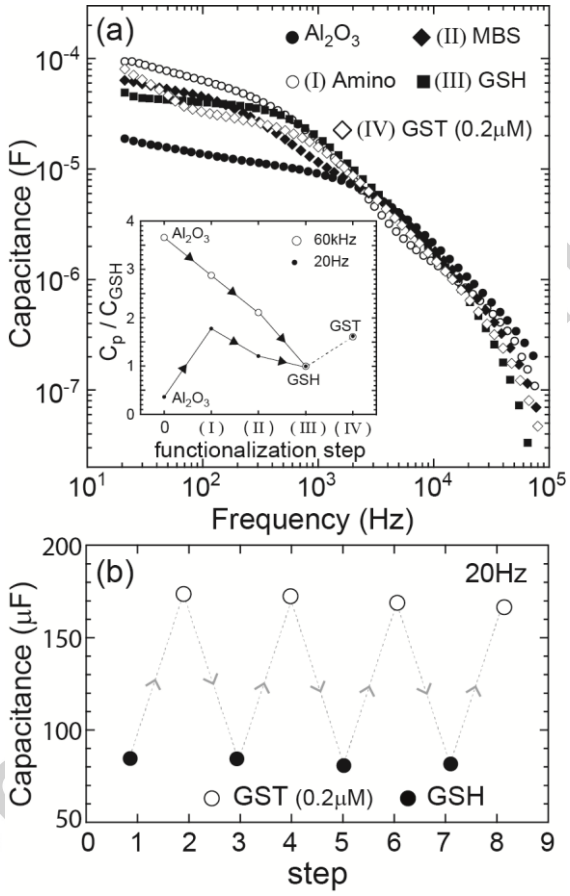

Fig. 3. (a) Frequency dependence of the measured capacitance as the functionalization steps evolve. All measurements were done after each respective functionalization step in a solution of 0.1 mol L^{-1} PBS at pH 7.0. The immobilization of the GST was performed in a 0.2 μmol L^{-1} solution. (inset) C_p normalized by C_{GSH}. at 20 Hz and 60 kHz for the sequential functionalization steps. (b) Variation of the capacitance for sequential immobilization and regeneration steps. The electrode area (A) is ~0.250 cm^2.

Fig. 3b exhibits the changes of the capacitance under immobilization (step IV in Fig. 2c) and regeneration steps (V), showing the reversibility of the GSH/GST interaction. This evaluation was carried out at 20 Hz. As previously described, the immobilization (odd-even steps in Fig. 3b) takes 1h a 0.2 μmol L^{-1} GST solution prepared in PBS. The regeneration (even-odd steps in Fig. 3b) was performed by washing the device in a 10 mmol L^{-1} GSH solution for 2 h. The regeneration of functional layer has been previously reported by Glatz et.al.(Glatz et al., 1997b), and most recently by Lin et.al. and de Oliveira et.al. (de Oliveira et al., 2016; Lin et al., 2004), where GST can be eluted using a highly concentrated GSH solution. This is possible because of the specific interaction between GSH and GST is more favored to occur with free GSH molecules in washing solution than with the immobilized ones. The capacitance changes shown in Fig. 3b varied up 6.5% when using the same device for detecting GST, whereas the response varied about 20% among four distinct biosensors. Such low variability of the biosensor response validates the effectiveness and reproducibility of the fabrication method. By following Fig. 3b, the variation of the net amount of positive charges at the electrode-electrolyte interface, due to the GSH/GST interaction (Q_{GST}), is in average 67±2 μC/cm^2. Finally, a similar evolution shown in Fig. 3b for capacitance values can also be observed for the measured resistance (see Section 5 and Fig. S5 in the Supplementary Material).

3.3 Reversible detection of GST at various concentrations

By repeating the same procedure employed to evaluate the reversibility of the detection process (Fig. 3b), the GSH/GST interaction was probed by varying the GST concentration from 200 pmol L^{-1} to 2μmol L^{-1}. For this experiment, an electrode area of ~ 0.15 cm^2 was employed. Since the biosensor surface can be easily regenerated, the same device was used for all assays. Fig. 4 shows the device capacitance at 20Hz as a function of the GST concentration. Each point

in the graph corresponds to a series of 4 consecutive immobilization/regeneration cycles. After each GST immobilization step (~1 h), the GSH capacitance value is fully recovered (C_{GSH} = 57.1±0.1μF). It is worth to mention that the data set shown in the Fig. 4a consist in a continuous increase of GST concentration, alternated with regeneration steps. Since the total capacitance is proportional to the whole amount of GST immobilized at the surface, we pointing out that the correlation between capacitance and GST concentration depends on both the regeneration time and the GST exposure time. The GST exposure time has to be kept constant regardless its concentration. If regeneration is not performed and the biosensor is exposed to new a GST concentration, the corresponding capacitance would be dependent on the availability of GSH sites. In this scenario, the measured capacitance will have an increment based on the value measured in the previous GST concentration. Finally, the hybrid functional structure endured a total of 28 immobilization/regeneration cycles. This fact demonstrates the robustness and stability of the device presented here. The capacitance changes, verified by varying the enzyme concentration, point out to a direct correlation between the amount of GST in solution and that at the device surface. Such correlation is better visualized by the difference $\Delta C = C_{GST} - C_{GSH}$ presented in Fig. 4b.

In Fig. 4b, the plot log(ΔC) *vs.* log[GST] indicates a linear operation regime (R^2=0.99) over 4 orders of magnitude. The red fitting line shown in the graph can be used as a reference curve for the biosensor operation. The biosensor shows a sensitivity of 0.2 F/mol.L^{-1} in a log-log calibration curve. Its response time (~ 10 min) corresponds to the time interval for the acquisition of an average of 90 capacitance readings. Faster acquisition of the biosensor response can be done in a timescale of 10s with lower accuracy on the measured capacitance.

The inset of Fig. 4b shows the evolution of Q_{GST} as a function of the concentration of GST. As the GST concentration increases, Q_{GST} tends to saturation, indicating that the structure is approaching the full surface molecular coverage at a given immobilization time. This regime also defines the upper detection limit of the sensor. The Q_{GST} *vs.* [GST] dependence, shown in the Fig. 4b inset, is better fit by a logarithmic function. Considering, in addition, an experimental error of ~2-3% (as obtained at 0.2 μmol. L^{-1}), we conclude that the upper detection limit for the device presented here may be set at ~2-10 μmol. L^{-1} of GST.

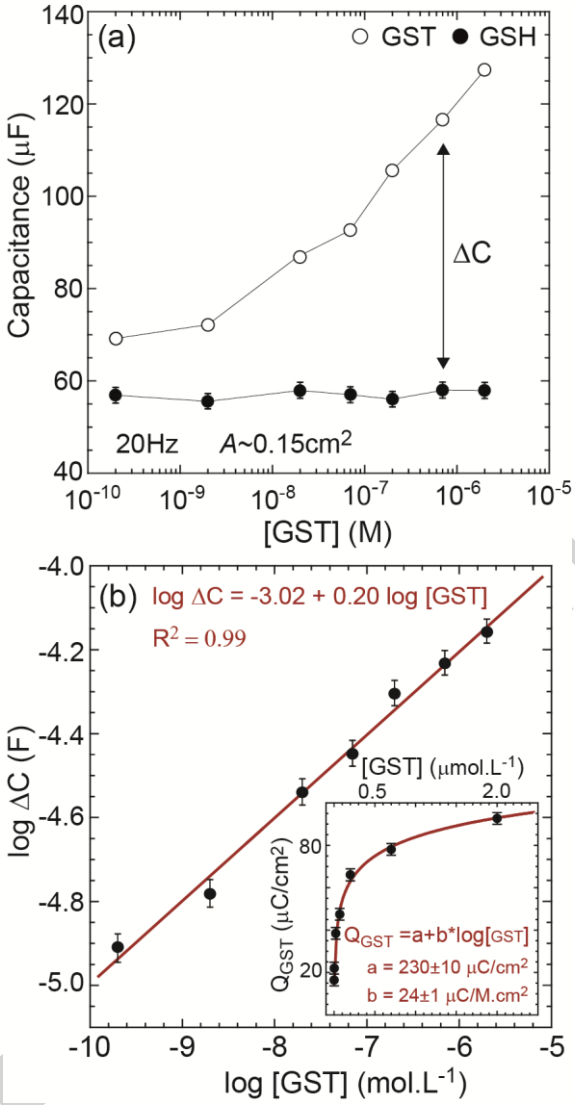

Fig.4. (a) Capacitance values after several immobilization/regeneration cycles. Full circles indicate the capacitance after surface regeneration with GSH. Open circles refer to the GST detection at different concentrations. The error bars are smaller than the size of the corresponding symbol. (b) Log (ΔC) versus log [GST] and variation of the net amount (ΔQ_{GST}) of positive charges due to the GSH/GST interaction (inset). The biosensor sensitivity is 0.2 F/mol L^{-1} in a log-log scale. The coefficient of variation is 6.5% Supporting electrolyte: 0.1 mol. L^{-1} PBS, pH 7.0. The electrode area (*A*) in this device is ~0.15 cm^2.

Finally, Table 1 shows a comparison between the performance of our device in respect to previously reported GST biosensors based on different platforms. Apart of being one of the few available reversible systems, the label-free hybrid biosensor is capable to detect GST at concentrations down to 200 pmol. L^{-1} – the lowest value reported according to the references. In addition, our device shows the broadest linear operation range, with response to GST concentrations over 4 orders of magnitude. To the best of our knowledge, this value is twice the highest value presented in literature for GST detection. The highest detectable concentration (2 μmol. L^{-1}) is in the same order of what has been reported by spectral surface plasmon resonance (Jung et al., 2006).

Table 1. Comparison of the main parameters in GST biosensors. LDV is the lowest detectable value and HDV the highest detectable value obtained from literature. The last row includes the values obtained in this work.

System	LDV (mol.L^{-1})	HDV (mol.L^{-1})	Reversible	Refs.
GSH/GST	2 x 10^{-9}	1 x 10^{-7}	Yes	[(Lin et al., 2009)]
GSH/GST	2.1 x 10^{-8}	4.2 x 10^{-6}	No	[(Jung et al., 2006)]
Ferrocene-glutathione/GST	-	9 x 10^{-7}	No	[(Martos-Maldonado et al., 2012)]
AuNc/AuNR-GSH/GST	2 x 10^{-9}	1 x 10^{-7}	No	[(Qin et al., 2015)]
GSH/GST	**2 x 10^{-10}**	**2 x 10^{-6}**	**Yes**	**This work**

4. Conclusion

In this work, we demonstrate the fabrication and characterization of a reversible label-free hybrid organic-inorganic nanostructured biosensor for the direct evaluation of biochemical interactions. The device's manufacture process combines standard microfabrication techniques

with self-assembly methods, highlighting the synergy between top-down and bottom-up approaches. The device performance also evidences the potentiality of nanostructured hybrid systems, which in our case involves materials and interfaces with different nature: organic-inorganic and solid-liquid. The functionalization route designed to immobilize the organic functional layer on top of the Al_2O_3 nanocoating is successfully demonstrated. The conditioning method applied to the oxide surface is effective to bring the stability necessary to continuously operate the device in aqueous medium. The device structure can be easily regenerated for repeating analysis. Such advantage reduces device-to-device measurement variations as well as manufacturing costs. Two figures-of-merit are substantially improved in this work considering other GST biosensors reported in literature: a) the linear operation range is two orders of magnitude (from 200 $pmol.L^{-1}$ to 2 $\mu mol.L^{-1}$ GST) broader, and b) the lowest detectable GST concentration is one order of magnitude smaller. Due to the high performance obtained during the monitoring of GSH/GST interaction through the relative charge variation at the solid(hybrid)/liquid interface, this platform may be of interest as screening biosensor for future studies of other biomolecular associations.

Acknowledgements

The authors acknowledge Angelo Luiz Gobbi, Maria Helena de Oliveira Piazzetta, Paulo Zambrozi Júnior e Rui César Murer for technical support during the microfabrication process. We also acknowledge Rafael Furlan de Oliveira for the fruitful discussions and suggestions. CAPES, CNPq (Project 483550/2013-2), FAPESP (Project 2013/22127-2) and FAPESP (Project 2014/ 25979-2) for the financial support.

Appendix A. Supplementary material.

Supplementary data associated with this article can be found in the online version at

http://dx.doi.org/.

References

Ahn, J.-H., Choi, S.-J., Han, J.-W., Park, T.J., Lee, S.Y., Choi, Y.-K., 2010. Double-Gate Nanowire Field Effect Transistor for a Biosensor. Nano Letters 10, 2934–2938. doi:10.1021/nl1010965

Ashkenasy, G., Cahen, D., Cohen, R., Shanzer, A., Vilan, A., 2002. Molecular Engineering of Semiconductor Surfaces and Devices. Accounts of Chemical Research 35, 121–128. doi:10.1021/ar990047t

Bard, A.J., Faulkner, L.R., 2000. Electrochemical Methods: Fundamentals and Applications, 2nd ed. Wiley.

Berggren, C., Bjarnason, B., Johansson, G., 2001. Capacitive Biosensors. Electroanalysis 13, 173–180.

Bof Bufon, C.C., Arias Espinoza, J.D., Thurmer, D.J., Bauer, M., Deneke, C., Zschieschang, U., Klauk, H., Schmidt, O.G., 2011. Hybrid Organic/Inorganic Molecular Heterojunctions Based on Strained Nanomembranes. Nano Lett. 11, 3727–3733. doi:10.1021/nl201773d

Bof Bufon, C.C., Cojal González, J.D., Thurmer, D.J., Grimm, D., Bauer, M., Schmidt, O.G., 2010. Self-Assembled Ultra-Compact Energy Storage Elements Based on Hybrid Nanomembranes. Nano Lett. 10, 2506–2510. doi:10.1021/nl1010367

Bousse, L., Bergveld, P., 1983. On the impedance of the silicon dioxide/electrolyte interface. Journal of Electroanalytical Chemistry and Interfacial Electrochemistry 152, 25–39. doi:10.1016/S0022-0728(83)80030-8

Casalini, S., Dumitru, A.C., Leonardi, F., Bortolotti, C.A., Herruzo, E.T., Campana, A., de Oliveira, R.F., Cramer, T., Garcia, R., Biscarini, F., 2015. Multiscale Sensing of Antibody–Antigen Interactions by Organic Transistors and Single-Molecule Force Spectroscopy. ACS Nano 9, 5051–5062. doi:10.1021/acsnano.5b00136

Casero, E., Darder, M., Pariente, F., Lorenzo, E., Martín-Benito, J., Vázquez, L., 2002. Thiol-Functionalized Gold Surfaces as a Strategy to Induce Order in Membrane-Bound Enzyme Immobilization. Nano Letters 2, 577–582. doi:10.1021/nl0255505

Chuang, S.-T., Chu, P., Sugimura, J., Tretiakova, M.S., Papavero, V., Wang, K., Tan, M., Lin, F., Teh, B.T., Yang, X.J., 2005. Overexpression of Glutathione S-Transferase a in Clear Cell Renal Cell Carcinoma. American Journal of Clinical Pathology 123, 421–429. doi:10.1309/AQXR6B2QPUGD638C

Cobben, P.L.H.M., Egberink, R.J.M., Bomer, J.G., Bergveld, P., Verboom, W., Reinhoudt, D.N., 1992. Transduction of selective recognition of heavy metal ions by chemically modified field effect transistors (CHEMFETs). Journal of the American Chemical Society 114, 10573–10582. doi:10.1021/ja00052a063

Correa, G.C., Bao, B., Strandwitz, N.C., 2015. Chemical Stability of Titania and Alumina Thin Films Formed by Atomic Layer Deposition. ACS Applied Materials & Interfaces 7, 14816–14821. doi:10.1021/acsami.5b03278

Cui, Y., 2001. Nanowire Nanosensors for Highly Sensitive and Selective Detection of Biological and Chemical Species. Science 293, 1289–1292. doi:10.1126/science.1062711

Daukantienė, L., Kazbarienė, B., Valuckas, K.P., Didžiapetrienė, J., Krikštaponienė, A., Aleknavičius, E., 2014. The significance of reduced glutathione and glutathione S-transferase during chemoradiotherapy of locally advanced cervical cancer. Medicina 50, 222–229. doi:10.1016/j.medici.2014.09.005

de Oliveira, R.F., Merces, L., Vello, T.P., Bof Bufon, C.C., 2016. Water-gated phthalocyanine transistors: Operation and transduction of the peptide–enzyme interaction. Organic Electronics 31, 217–226. doi:10.1016/j.orgel.2016.01.041

Finklea, H.O., Snider, D.A., Fedyk, J., Sabatani, E., Gafni, Y., Rubinstein, I., 1993. Characterization of octadecanethiol-coated gold electrodes as microarray electrodes by cyclic voltammetry and ac impedance spectroscopy. Langmuir 9, 3660–3667. doi:10.1021/la00036a050

Gao, X.P.A., Zheng, G., Lieber, C.M., 2010. Subthreshold Regime has the Optimal Sensitivity for Nanowire FET Biosensors. Nano Letters 10, 547–552. doi:10.1021/nl9034219

Glatz, Z., Psotová, J., Janiczek, O., Chroust, K., Jowet, T., 1997a. Use of thiopropyl sepharose for the synthesis of an adsorbent for the affinity chromatography of glutathione S-transferase. J. Chromatogr. B Biomed. Sci. Appl. 688, 239–243.

Glatz, Z., Psotová, J., Janiczek, O., Chroust, K., Jowet, T., 1997b. Use of thiopropyl Sepharose for the synthesis of an adsorbent for the affinity chromatography of glutathione S-transferase. Journal of Chromatography B: Biomedical Sciences and Applications 688, 239–243. doi:10.1016/S0378-4347(96)00267-8

Góes, M.S., Rahman, H., Ryall, J., Davis, J.J., Bueno, P.R., 2012. A Dielectric Model of Self-Assembled Monolayer Interfaces by Capacitive Spectroscopy†. Langmuir 28, 9689–9699. doi:10.1021/la301281y

Grimm, D., Bof Bufon, C.C., Deneke, C., Atkinson, P., Thurmer, D.J., Schäffel, F., Sandeep Gorantla, Bachmatiuk, A., Schmidt, O.G., 2013. Rolled-up nanomembranes as compact 3D architectures for field effect transistors and fluidic sensing applications. Nano Letters 13, 213–218. doi:10.1021/nl303887b

Groner, M.D., Fabreguette, F.H., Elam, J.W., George, S.M., 2004. Low-temperature Al2O3 atomic layer deposition. Chem. Mat. 16, 639–645. doi:10.1021/cm0304546

Hanson, E.L., Schwartz, J., Nickel, B., Koch, N., Danisman, M.F., 2003. Bonding Self-Assembled, Compact Organophosphonate Monolayers to the Native Oxide Surface of Silicon. Journal of the American Chemical Society 125, 16074–16080. doi:10.1021/ja035956z

Howie, A., Miller, W., Hawkins, R., Hutchinson, A., Beckett, G., 1989. Expression of glutathione S-transferase B1, B2, Mu and Pi in breast cancers and their relationship to oestrogen receptor status. British Journal of Cancer 60, 834–837. doi:10.1038/bjc.1989.375

Jung, J.-W., Jung, S.-H., Kim, H.-S., Yuk, J.S., Park, J.-B., Kim, Y.-M., Han, J.-A., Kim, P.-H., Ha, K.-S., 2006. High-throughput analysis of GST-fusion protein expression and activity-dependent protein interactions on GST-fusion protein arrays with a spectral surface plasmon resonance biosensor. PROTEOMICS 6, 1110–1120. doi:10.1002/pmic.200500371

Kapoli, P., Axarli, I.A., Platis, D., Fragoulaki, M., Paine, M., Hemingway, J., Vontas, J., Labrou, N.E., 2008. Engineering sensitive glutathione transferase for the detection of xenobiotics. Biosensors and Bioelectronics 24, 498–503. doi:10.1016/j.bios.2008.06.037

Lai, W.-A., Lin, C.-H., Yang, Y.-S., Lu, M.S.-C., 2012. Ultrasensitive and label-free detection of pathogenic avian influenza DNA by using CMOS impedimetric sensors. Biosensors and Bioelectronics 35, 456–460. doi:10.1016/j.bios.2012.02.049

Lin, S.-P., Pan, C.-Y., Tseng, K.-C., Lin, M.-C., Chen, C.-D., Tsai, C.-C., Yu, S.-H., Sun, Y.-C., Lin, T.-W., Chen, Y.-T., 2009. A reversible surface functionalized nanowire transistor to study protein–protein interactions. Nano Today 4, 235–243. doi:10.1016/j.nantod.2009.04.005

Lin, Y., Lu, F., Tu, Y., Ren, Z., 2004. Glucose Biosensors Based on Carbon Nanotube Nanoelectrode Ensembles. Nano Letters 4, 191–195. doi:10.1021/nl0347233

Liu, H., Peng, J., Gao, J., Zheng, F., Tie, C., 2015. Glutathione S-transferase T1 and M1 null genotypes and Parkinson's disease risk: evidence from an updated meta-analysis. Neurological Sciences 36, 1559–1565. doi:10.1007/s10072-015-2159-4

Liu, Y., Dong, X., Chen, P., 2012. Biological and chemical sensors based on graphene materials. Chem. Soc. Rev. 41, 2283–2307. doi:10.1039/C1CS15270J

Martos-Maldonado, M.C., Casas-Solvas, J.M., Téllez-Sanz, R., Mesa-Valle, C., Quesada-Soriano, I., García-Maroto, F., Vargas-Berenguel, A., García-Fuentes, L., 2012. Binding properties of ferrocene–glutathione conjugates as inhibitors and sensors for glutathione S-transferases. Biochimie 94, 541–550. doi:10.1016/j.biochi.2011.09.003

Martos-Maldonado, M.C., Casas-Solvas, J.M., Vargas-Berenguel, A., García-Fuentes, L., 2015. Electrochemical Detection of Glutathione S-Transferase: An Important Enzyme in the Cell Protective Mechanism Against Oxidative Stress, in: Armstrong, D. (Ed.), Advanced Protocols in Oxidative Stress III. Springer New York, New York, NY, pp. 123–138.

Materon, E.M., Jimmy Huang, P.-J., Wong, A., Pupim Ferreira, A.A., Sotomayor, M.D.P.T., Liu, J., 2014. Glutathione-s-transferase modified electrodes for detecting anticancer drugs. Biosensors and Bioelectronics 58, 232–236. doi:10.1016/j.bios.2014.02.070

Maupas, H., Soldatkin, A.P., Martelet, C., Jaffrezic-Renault, N., Mandrand, B., 1997. Direct immunosensing using differential electrochemical measurements of impedimetric variations. Journal of Electroanalytical Chemistry 421, 165–171. doi:10.1016/S0022-0728(96)04837-1

Mazzetti, A.P., Fiorile, M.C., Primavera, A., Lo Bello, M., 2015. Glutathione transferases and neurodegenerative diseases. Neurochemistry International 82, 10–18. doi:10.1016/j.neuint.2015.01.008

Nguyen, C.V., Delzeit, L., Cassell, A.M., Li, J., Han, J., Meyyappan, M., 2002. Preparation of Nucleic Acid Functionalized Carbon Nanotube Arrays. Nano Letters 2, 1079–1081. doi:10.1021/nl025689f

Qin, L., He, X., Chen, L., Zhang, Y., 2015. Turn-on Fluorescent Sensing of Glutathione *S* -Transferase at near-Infrared Region Based on FRET between Gold Nanoclusters and Gold Nanorods. ACS Applied Materials & Interfaces 7, 5965–5971. doi:10.1021/acsami.5b00269

Shan, C., Yang, H., Song, J., Han, D., Ivaska, A., Niu, L., 2009. Direct Electrochemistry of Glucose Oxidase and Biosensing for Glucose Based on Graphene. Analytical Chemistry 81, 2378–2382. doi:10.1021/ac802193c

Sharma, R., Bufon, C.C.B., Grimm, D., Sommer, R., Wollatz, A., Schadewald, J., Thurmer, D.J., Siles, P.F., Bauer, M., Schmidt, O.G., 2014. Large-Area Rolled-Up Nanomembrane Capacitor Arrays for Electrostatic Energy Storage. Advanced Energy Materials 4, n/a–n/a. doi:10.1002/aenm.201301631

Singh, R.P., Kim, Y.J., Oh, B.-K., Choi, J.-W., 2009. Glutathione-s-transferase based electrochemical biosensor for the detection of captan. Electrochemistry Communications 11, 181–185. doi:10.1016/j.elecom.2008.11.003

Stern, E., Klemic, J.F., Routenberg, D.A., Wyrembak, P.N., Turner-Evans, D.B., Hamilton, A.D., LaVan, D.A., Fahmy, T.M., Reed, M.A., 2007. Label-free immunodetection with CMOS-compatible semiconducting nanowires. Nature 445, 519–522. doi:10.1038/nature05498

Taylor, D.M., Macdonald, A.G., 1987. AC admittance of the metal/insulator/electrolyte interface. Journal of Physics D: Applied Physics 20, 1277–1283. doi:10.1088/0022-3727/20/10/010

Townsend, D.M., Tew, K.D., 2003. The role of glutathione-S-transferase in anti-cancer drug resistance. Oncogene 22, 7369–7375. doi:10.1038/sj.onc.1206940

Tsouti, V., Boutopoulos, C., Zergioti, I., Chatzandroulis, S., 2011. Capacitive microsystems for biological sensing. Biosensors and Bioelectronics 27, 1–11. doi:10.1016/j.bios.2011.05.047

Tsuchida, S., Sato, K., 1992. Glutathione Transferases and Cancer. Critical Reviews in Biochemistry and Molecular Biology 27, 337–384. doi:10.3109/10409239209082566

Vervacke, C., Bof Bufon, C.C., Thurmer, D.J., Schmidt, O.G., 2014. Three-dimensional chemical sensors based on rolled-up hybrid nanomembranes. RSC Advances 4, 9723. doi:10.1039/c3ra47200k

Vervacke, C., Bof Bufon, C.C., Thurmer, D.J., Siles, P.F., Schmidt, O.G., 2012. High-Performance Organic Nanomembrane Based Sensors for Rapid in Situ Acid Detection. Analytical Chemistry 84, 8399–8406. doi:10.1021/ac301959e

Zheng, G., Patolsky, F., Cui, Y., Wang, W.U., Lieber, C.M., 2005. Multiplexed electrical detection of cancer markers with nanowire sensor arrays. Nature Biotechnology 23, 1294–1301. doi:10.1038/nbt1138

Highlights

- Hybrid organic-inorganic functional layer to monitor biospecific interactions.
- Reversible label-free glutathione-S-transferase (GST) biosensor.
- Four orders of magnitude wide detectable GST concentration.
- Low detectable GST concentration (200 pmol.L-1).